Determination of the crystal field and nature of x-ray linear dichroism for Co-O with local octahedral, tetrahedral, and tetragonal symmetries

M. Wu,[1,*] X. Huang,[2] K. H. L. Zhang,[2] S. Hu,[3] L. Chen,[3] H.-Q. Wang,[1,†] and J. Kang[1]

[1]*Fujian Provincial Key Laboratory of Semiconductors and Applications, Collaborative Innovation Center for Optoelectronic Semiconductors and Efficient Devices, Department of Physics, Xiamen University, Xiamen, 361005, People's Republic of China*

[2]*State Key Laboratory of Physical Chemistry of Solid Surfaces, College of Chemistry and Chemical Engineering, Xiamen University, Xiamen 361005, People's Republic of China*

[3]*Department of Physics, Southern University of Science and Technology, Shenzhen, Guangdong 518055, People's Republic of China*

(Received 24 May 2021; accepted 28 July 2021; published 6 August 2021)

Cobalt oxides with multiple local Co-O coordination environments such as octahedral, tetrahedral, and tetragonal networks display versatile electronic and magnetic properties which have attracted great interest in many fields. Understanding the ground-state properties and determining the fundamental band gap remain challenges in cobalt-based compounds and thin films, which have been investigated here using synchrotron-based Co L_{23}-edge x-ray absorption measurements followed by configuration interaction cluster calculations. We focus on the detailed Co L_{23}-edge absorption spectral variations in different octahedral crystal fields as well as in the less investigated tetrahedral and tetragonal systems, taking into account Co ions with different valence states. From a quantitative comparison between the simulated spectrum and an accurately measured absorption spectrum of a specified compound, the crystal field value can be extracted from the Co L_{23}-edge absorption spectrum, which is complementary to the results obtained in optical measurements and other calculations. Furthermore, Co L_{23}-edge x-ray linear dichroism shows the same spectral evolutions as a result of either local CoO_6 cluster with tetragonal symmetry or the magnetic exchange field, whereas both coexist in most antiferromagnetic cobalt oxide thin films. Detailed temperature and polarization-dependent Co L_{23}-edge absorption measurements have been proposed to distinguish both contributions, which show different spectral variations due to the specified modifications of the ground and final states at different temperatures. Our results offer theoretical guidance for understanding the multiplet structure of Co L_{23}-edge absorption spectrum, obtaining the precise crystal field value for cobalt oxides with versatile coordinations, and explaining the underlying mechanism of x-ray linear dichroism, as well as understanding the fundamental physical properties and their potential applicability of cobalt oxides and their thin films.

DOI: 10.1103/PhysRevB.104.075109

I. INTRODUCTION

Cobalt oxides are of particular interest due to their diverse magnetic, electronic, and optical properties [1–3] as well as due to their rich technological applications such as solid oxide fuel cells, oxidization catalysts, gas sensors, and membranes for oxygen separation [4–7], etc. Among them, two representative classes of cobalt oxides are the spinel Co_3O_4 structural compounds where the variation of the cations on octahedrally and tetrahedrally coordinated sites can be used to tune the ground-state properties determining the potential optoelectronic applications [8–10] and the $ACoO_3$ (A=Alkaline earth metal or lanthanide) perovskite compounds where the complicated phase diagram can be strongly modified by the A site cations with different ionic radii [3,11,12], as will be focused on below. In the ionic limit, cobalt cations can adopt multiple valence states with Co^{2+}, Co^{3+}, and Co^{4+}, corresponding to Co $3d^7$, Co $3d^6$, and Co $3d^5$ electronic configurations, respectively. Moreover, cobalt ions are susceptible to multiple spin states. Both diverse valence states and multiple spin states serve as the driving forces for the aforementioned distinct physical properties.

Most cobalt oxides exhibit insulating behaviors while the origin of the band gap remains controversial. Depending on the competition between electron-electron Coulomb interaction energy U_{dd} and the charge transfer energy Δ representing the charge fluctuation energy to move one electron from the ligand hole $\underline{L}$ to the Co $3d$ site, the band gap can be forms of the $p-d$ type, composed of different kinds of orbitals or the $d-d$ type due to Coulomb interaction [13]. For spinel Co_3O_4 and the isostructural compounds, the determination of the fundamental band gap is more complicated due to the coexistence of local octahedral and tetrahedral networks. For example, the value of the band gap in Co_3O_4 is still under debate and remains elusive, which has been reported as 2.2, 1.6, 1.2, or 0.76 eV in literature [14–16]. Our recent work reported a fundamental band gap of ~0.8 eV in Co_3O_4 epitaxial thin film using combined x-ray spectroscopies, optical spectroscopy and theoretical calculations, which can be ascribed to the tetrahedrally coordinated Co^{2+} cations [10]. Aiming

*meng.wu@xmu.edu.cn
†hqwang@xmu.edu.cn

for providing a fundamental understanding of the ground-state properties and, in particular, the crystal field splitting of cobalt oxide compounds which is important for clarifying the band gap issue, here we performed configuration interaction (CI) cluster calculations considering Co-O clusters with octahedral and tetrahedral networks, using experimentally measured Co L_{23}-edge absorption spectra of perovskite and spinel structures as fingerprints.

Furthermore, accompanying the demand for miniaturization of electronic materials and the fast development of thin-film deposition techniques, transition metal thin films have expanded into a booming field. Strain engineering has been proven as one of the efficient external stimuli in tuning novel electronic properties, which generally can lower the crystal symmetry. We thus performed CI cluster calculations considering a CoO_6 cluster with tetragonal symmetry to understand the multiplet effects and the ground-state properties. X-ray linear dichroism originating from the spectral difference of different linearly polarized x-ray beams is expected due to the anisotropic electron occupations in different orbitals within the tetragonal crystal field. However, the linear dichroic effect is more complicated for common antiferromagnetic Co-based thin films since here magnetic exchange interaction gives rise to the same linear dichroism as lowering of the crystal symmetry from cubic to tetragonal. The question is how to separate the contributions from magnetic exchange field and tetragonal crystal field as well as to clarify the fundamental ground-state properties. Based on our CI cluster calculations, further temperature- and polarization-dependent absorption measurements have been suggested to distinguish the aforementioned two contributions, as will be presented in detail below.

In this paper, experimentally measured Co L_{23}-edge absorption spectra have been used as fingerprints to understand the multiplet structures based on CI cluster calculations considering Co-O clusters of different electronic configurations. In the following, we present the simulated absorption spectra at Co L_{23}-edge for Co $3d^7$, Co $3d^6$, and Co $3d^5$ electronic configurations with local octahedral coordination environment in Sec. III A and with tetrahedral symmetry in Sec. III B. From a comparison between the simulated spectrum and the measured absorption spectrum of a specified compound, we can extract the ground-state properties and the crystal field splitting energy. In Sec. III C, the Co L_{23}-edge absorption spectra with tetragonal symmetry are calculated, where the natural linear dichroism has been observed due to the anisotropic symmetries of $3d$ orbitals and the strict parity selection rules. We focus on the linear dichroic effect in Sec. III D and show that the magnetic exchange field may bring the same linear dichroism as lowering the crystal symmetry from cubic to tetragonal. Further temperature, and polarization-dependent absorption measurements have been proposed to distinguish both contributions. Finally, the conclusion.

II. EXPERIMENTAL AND COMPUTATIONAL DETAILS

Synchrotron-based transition metal L_{23}-edge x-ray absorption measurement is an element-specified method showing strong sensitivity to the ground-state properties such as valence state of transition metal ions, magnetic exchange field, orbital occupations under different symmetries, and crystal field splitting as well as spin-orbit coupling, etc. To have the experimentally measured Co L_{23}-edge absorption spectra as fingerprints for CI cluster calculations, we grew high quality epitaxial $ZnCo_2O_4$, $CoAl_2O_4$, and $SrCrO_3$ thin films by pulsed laser deposition technique. Spinel $ZnCo_2O_4$ and $CoAl_2O_4$ thin films with thicknesses of ∼30 nm were deposited on (001)-oriented $MgAl_2O_4$ substrates (see Ref. [10] for details). The Co L_{23}-edge x-ray absorption spectra of $ZnCo_2O_4$ thin films with Co^{3+} $3d^6$ in octahedral symmetry as well as $CoAl_2O_4$ with Co^{2+} $3d^7$ in tetrahedral symmetry were performed at the soft x-ray beamline, Australian Synchrotron [10]. High quality epitaxial $SrCoO_3$ thin film has been deposited on the (001)-oriented $SrTiO_3$ substrate with a thickness of ∼10 nm (see Ref. [17] for experimental details). The absorption spectrum of $SrCoO_3$ thin film with Co^{4+} $3d^5$ electronic configuration in octahedral symmetry was measured at beamline 4B9B of the Beijing Synchrotron Radiation Facility [17].

However, understanding the transition metal L_{23}-edge absorption spectrum is difficult since multiplet effects arising from the overlap between the core state and valence state electron wave functions are important. The transition probabilities calculated by first principles calculations are inadequate for transition metal L_{23}-edge absorption spectrum based on a single particle model. Therefore, the theory for CI calculation of a transition metal-oxygen cluster was established years ago, which shows the advantages in providing a quantitative description of L_{23}-edge absorption spectrum based on a many-body electron basis. We refer to the literature as well as our previous reports for the backgrounds and details on performing CI cluster calculations [18–23]. Note that the energy parameters here are calculated by constructing single-particle molecular orbitals as linear combinations of atomic Hartree-Fock orbitals, rather than the orbitals obtained from *ab initio* band-structure calculations. In this paper, CI cluster calculations considering Co-O clusters of different electronic configurations were performed. The splitting of different energy levels for Co and oxygen ions arranged in octahedral, tetrahedral, and tetragonal networks due to crystal field effects are illustrated in Fig. 1. The energy parameters denoting the crystal field splitting are Δ_o and Δ_t for octahedral and tetrahedral symmetries, respectively. The tetragonal distortion can be modeled by two additional energy parameters, i.e., Δ_{eg} and Δ_{t2g}, denoting the energy differences between $d_{3z^2-r^2}$ and $d_{x^2-y^2}$, as well as between $d_{xz,yz}$ and d_{xy} levels, respectively. We used $\Delta_{eg} = 2\Delta_{t2g}$ in the first approximation in the present calculations to account for the anisotropic hybridization strengths between e_g and t_{2g} orbitals since the hopping magnitude of e_g-O $2p$ orbitals is twice as large as that of the t_{2g}-O $2p$ orbitals.

III. RESULTS AND DISCUSSIONS

A. CoO_6 cluster with octahedral symmetry (O_h)

We used the experimentally measured Co L_{23}-edge absorption spectra of different electronic configurations as fingerprints, i.e., CoO with Co^{2+} $3d^7$ [24], perovskite $EuCoO_3$ [25] and spinel $ZnCo_2O_4$ compounds with Co^{3+} $3d^6$ [10], as well

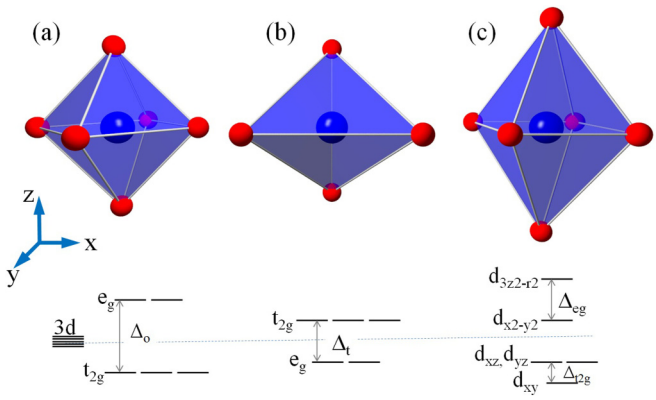

FIG. 1. Schematic views of transition metal ion Co surrounded by O ions with (a) octahedral, (b) tetrahedral, and (c) tetragonal symmetry. Illustrations of the corresponding energy level diagram in presence of different crystal field are shown below. Δ_o and Δ_t represent the energy splitting between t_{2g} and e_g orbitals in octahedral and tetrahedral symmetries, respectively. Two energy parameters Δ_{eg} and Δ_{t2g} have been used to model the tetragonal crystal field effect.

as $SrCoO_3$ compounds with Co^{4+} $3d^5$ electronic configurations [17]. The features of the measured spectra can be well captured in the simulated spectra shown as bold curves in Figs. 2(a)–2(c) at specific Δ_o values, i.e., $\Delta_o \sim 0.6$ eV for CoO, $\Delta_o \sim 0.8$ eV for $EuCoO_3$ and $ZnCo_2O_4$, and $\Delta_o \sim 0.6$ eV for $SrCoO_3$. These octahedral crystal field splitting

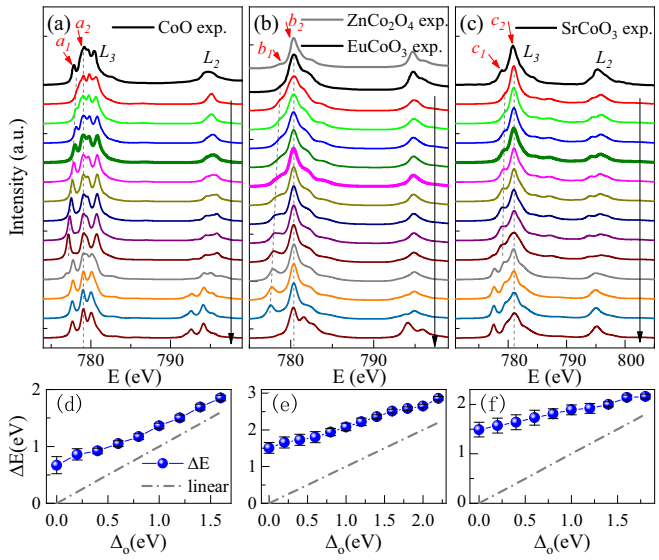

FIG. 2. The calculated isotropic spectra with a variation of Δ_o within the range between 0 and 2.4 eV from top to bottom, in comparison with the experimental measured Co L_{23}-edge absorption spectra for (a) Co $3d^7$ [24], (b) Co $3d^6$ [10,25], and (c) Co $3d^5$ [17]. The bold curves denote the spectra showing the best agreement with the experimental spectra at specific Δ_o values. The rest of the energy parameters are shown in Table I. Grey dashed lines are guided for eyes with gradual increase of splitting. Panels (d)–(f) show the corresponding peak splitting ΔE versus different Δ_o values. The grey dot-dashed line in each panel displays the condition that the peak energy splitting ΔE is equal to Δ_o.

values are comparable to the results reported in literature from other calculations or experiments [10,24,26–28]. The rest of the energy parameters are listed in Table I. The Slater parameters used in the present calculations are scaled to 80% of the values for a free ion, taking into account the intra-atomic CI inside a solid. For CoO (Co^{2+} $3d^7$ O_h), similar U_{dd} and Δ values have been reported before [13,26,29]. The comparable U_{dd} and Δ values imply that the band gap is an intermediate character between the charge-transfer and Mott Hubbard regimes and a dominant $3d^7$ electronic configuration. The smaller Δ value compared to U_{dd} for Co^{3+} in $EuCoO_3$ and $ZnCo_2O_4$ compounds suggests that the band gap is of $p-d$ type, making them charge transfer insulators. Recently, an optical band gap of $p-d$ charge transfer type was reported by Samanta, using full potential linearized augmented plane wave method based on the density functional theory(DFT) [30]. In comparison of the best-fitting energy parameters obtained from present calculations as shown in Table I, a decrease of the charge transfer energy value Δ as Co going from Co^{2+} to Co^{4+} is visible, which is related to the decrease of formal $3d$ electron number and the lowering of the $3d$ orbitals. Potze *et al.* reported comparable energy values in $SrCoO_3$ compound in atomic-multiplet calculations [28]. The $SrCoO_3$ compound with a negative Δ value indicates a strong covalent effect and the ground state is dominant by the ligand hole character with $3d^6\underline{L}$ electronic configuration, i.e., the nominal charge state is not Co^{4+} but strongly compensated by O $2p$ holes.

CI calculations for CoO_6 octahedron with cubic symmetry have been performed for different Co electronic configurations with the crystal field Δ_o as the only free parameter. Figures 2(a)–2(c) exhibit the calculated absorption spectra with a variation of the crystal field splitting value Δ_o from 0 to 2.4 eV at an interval of 0.2 eV from top to bottom spectra. Globally, an expansion of the multiplet structure is suggested as Δ_o increases due to the increased energy splitting between t_{2g} and e_g energy levels. At high Δ_o values, abrupt changes in the spectra are visible, indicating high-spin to low-spin state transitions. With cubic symmetry, the $3d$ orbitals are split into lower-lying t_{2g} orbitals with threefold degeneracy and high-lying e_g orbitals with twofold degeneracy. With small octahedral crystal fields, Co ions favor the occupation of t_{2g} orbitals. Hund's rule tends to align the spins parallel, leading to the high spin electronic configuration as the ground state. However, for larger Δ_o values, the crystal field exceeds the energy gain of spin pairing, Hund's rule is broken and the spin configuration changes to low-spin. The spin state transition appears at $\Delta_o \sim 1.8$ eV for Co $3d^7$, $\Delta_o \sim 2.4$ eV for Co $3d^6$, and $\Delta_o \sim 1.4$ eV for Co $3d^5$, considering the full multiplet interactions. We note that the crystal field values appearing in the spin-state transitions are comparable to these proposed in literature, i.e., Δ_o between 1.5 eV to 2 eV for Co $3d^7$ [31], Δ_o between 2 eV to 2.5 eV for Co $3d^6$ [31], and $\Delta_o \sim 1.2$ eV for Co $3d^5$ in $SrCoO_3$ compound [28].

We further extract the peak splitting ΔE, i.e., the energy differences between peaks a_1 and a_2 for Co $3d^7$, peaks b_1 and b_2 for Co $3d^6$, peaks c_1 and c_2 for Co $3d^5$ at the L_3 edge, versus different Δ_o values, as shown in Figs. 2(d)–2(f). ΔE is clearly deviated from the grey dot-dashed line representing the same energy value between the energy splitting at the L_3 edge

TABLE I. List of the values used for present CI calculations of different electronic configurations, including the F^2_{dd} and F^4_{dd} Slater parameters for $d-d$ interactions, the F^2_{pd}, G^1_{pd} and G^3_{pd} Slater integrals for $p-d$ interactions, the $d-d$ Coulomb interaction U_{dd}, the attractive interaction U_{pd} between the core hole and the $3d$ electron, the charge transfer energy Δ representing the energy required to move one electron from the ligand to Co $3d$ site, as well as the hopping magnitude expressed in terms of Slater-Koster parameters $pd\sigma$ and $pd\pi$, with $pd\sigma/pd\pi$=2.17 reflecting the anisotropic hybridization strengths. All the values are in unit of eV.

Configuration	F^2_{dd}	F^4_{dd}	F^2_{pd}	G^1_{pd}	G^3_{pd}	U_{dd}	U_{pd}	Δ	pdσ
$Co^{2+}3d^7O_h$	12.395	7.707	7.259	5.349	3.068	6.5	8.2	6.5	1.2
$Co^{3+}3d^6O_h$	13.421	8.394	7.899	5.947	3.384	5.5	7.0	2.0	0.5
$Co^{4+}3d^5O_h$	14.372	9.034	8.544	6.525	3.716	7.5	9.8	−2.0	1.2
$Co^{2+}3d^7T_d$	12.395	7.707	7.259	5.349	3.068	6.5	8.2	4.0	0.5

and crystal field parameter Δ_o. The peak splitting ΔE shows a monotonic increase as Δ_o increases, which can be used as an energy parameter to evaluate the crystal field parameter, but not directly equal to Δ_o in magnitude. Crystal field splitting Δ_o exhibits as one of the crucial parameters in determining the optoelectronic properties. From a quantitative comparison of the simulated spectrum to an accurately measured absorption spectrum of a specified compound, one can extract the crystal field strength Δ_o from Co L_{23}-edge soft x-ray absorption spectrum, which is complementary to the results obtained from optical measurements and provides a benchmark for choosing the proper $e-e$ Coulomb interaction energy U_{dd} value in other theoretical calculations [32,33].

B. CoO_4 cluster with tetrahedral symmetry (T_d)

Tetrahedral coordinated Co exists as one of the important structural ingredients in cobalt oxides,e.g., the layered cobaltates family such as $YBaCo_4O_7$ composed of kagome layers of tetrahedrally coordinated Co [34] and the Co-based spinel family containing both the tetrahedral and octahedral sites such as Co_3O_4 and $CoAl_2O_4$, etc. [10]. However, CI calculations only have been intensively studied for CoO_6 clusters with local octahedral coordination, but much less for the tetrahedral case. CI calculations thus have been performed to exam the influences of tetrahedral crystal field Δ_t on the absorption spectra for a CoO_4 cluster with different Co valence states. We have not found the absorption spectra for Co^{6+} and Co^{5+} with local tetrahedral symmetries in literature, to the best of our knowledge. Figure 3(a) shows the experimental measured Co L_{23}-edge absorption spectra for $CoAl_2O_4$ with Co $3d^7$ electronic configuration in tetrahedral symmetry [10]. Our cluster calculation with the best-fitting energy parameters can reproduce the experimental spectrum well, shown as the bold curve with $\Delta_t \sim 0.8$ eV in Fig. 3(a). The other parameters are also included in Table I. This tetrahedral crystal field of ~0.8 eV for $CoAl_2O_4$ obtained from Co L_{23}-edge absorption spectrum is comparable to the results suggested from optical absorption measurement, as reported in our recent paper [10].

Figures 3(a)–3(c) show the calculated absorption spectra at different tetrahedral crystal field splitting values, i.e., Δ_t from 0 to 2.0 eV at an interval of 0.2 eV. Overall, the spectral evolutions Co $3d^7$ and Co $3d^6$ as Δ_t increases are similar to the spectra reported by van der Laan. However, their calculated spectra are lacking reproduction of the full multiplet structures since only the transition probability in the form of $3d^n \rightarrow 2p^5 3d^{n+1}$ has been considered [31]. For Co $3d^7$, dramatic variations of the spectra have been observed as Δ_t increases from 0 to 1.0 eV. We note that for Co $3d^7$, only one spin configuration $e_g^{2\uparrow} e_g^{2\downarrow} t_{2g}^{3\uparrow}$ is allowed and no spin-state transition thus is expected. The multiplet structures are related to the spin-orbit coupling of the Co^{2+} ions. For Co $3d^6$ and Co $3d^5$ with tetrahedral symmetry, the energy parameters used for the absorption spectra calculated for tetrahedral symmetry are the same as these used for octahedral symmetry. The spectra for zero crystal field corresponding to a spherical symmetry are identical for both octahedral and tetrahedral coordination environments. With Δ_t increasing, we observe a splitting of the excitation peaks, which are marked as black arrows in Figs. 3(b) and 3(c), indicative of an enhanced tetrahedral crystal field splitting. We further note that a linear combination of CI simulated spectra with different Co valence states in octahedral and tetrahedral symmetries can be used to capture the experimental absorption spectrum of a spinel structure with integer and even with mixed valence states in both octahedral and tetrahedral sites [35]. This is favorable since depending on the material synthesis conditions, spinel Co oxide with mixed valence states is common in practical cases, which determines the multifunctional physical behaviors and applications.

C. CoO_6 with tetragonal symmetry

In this section, we further consider the CI calculated spectra for CoO_6 under a local tetragonal symmetry for Co ions of

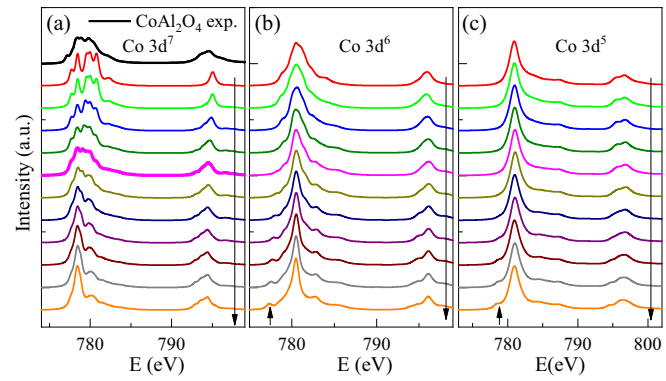

FIG. 3. The calculated isotropic spectra with a variation of tetrahedral crystal field Δ_t between 0 and 2 eV from top to bottom for (a) Co $3d^7$, (b) Co $3d^6$ and (c) Co $3d^5$ electronic configurations. The rest of the energy parameters are listed in Table I. The experimental measured Co L_{23}-edge absorption spectrum for $CoAl_2O_4$ with Co $3d^7$ in tetrahedral symmetry [10] was used as a fingerprint for calculations. The bold curve in panel (a) represents the spectrum with the best reproduce of the experimental spectrum with $\Delta_t \sim 0.8$ eV.

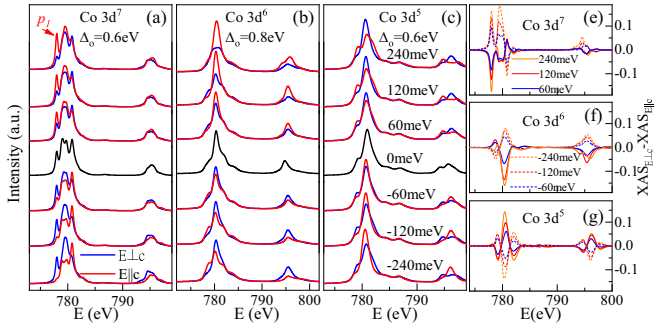

FIG. 4. The calculated Co L_{23}-edge absorption spectra for $E \perp c$ and $E \parallel c$ incoming photon polarizations at different crystal field splitting values, i.e., Δ_{t2g} of 240 meV, 120 meV, 60 meV, 0 meV, −60 meV, −120 meV, and −240 meV from top to bottom spectra, for (a) Co $3d^7$, (b) Co $3d^6$, and (c) Co $3d^5$ electronic configurations, respectively. Panels (e) and (f) show the corresponding linear dichroic spectra, i.e., ($XAS_{E\perp c} - XAS_{E\parallel c}$) at different Δ_{t2g} values.

different electronic configurations. A lowering of the crystal symmetry from cubic to tetragonal is particularly useful for strain engineering of functional oxide thin films, which has been verified as an effective approach to tailor the electronic properties in strongly correlated transition metal oxide thin films [36–38]. For CoO_6 coordination complex under tetragonal symmetry, the e_g (t_{2g}) manifold further splits into $d_{x^2-y^2}$ and $d_{3z^2-r^2}$ (d_{xz}, d_{yz} and d_{xy}) orbitals. In responses of the different in-plane stress, reorientations of the spin direction and orbital momentum may appear [39,40]. Due to the anisotropic nature of the orbitals, the selection rules restrict the dipole allowed transition in certain manners. X-ray linear dichroism, i.e., the probe of the solid with different linearly polarized electromagnetic waves, shows the sensitivity to the orbitals of the transition metal ion under different local symmetries, the corresponding orbital occupations and the orbital response to lattice variations for a particular ion.

To model the crystal field effect under tetragonal symmetry, three parameters, i.e., Δ_o, Δ_{eg} and Δ_{t2g}, are necessary as shown in Fig. 1(c). For the energy difference between t_{2g} and e_g levels, we used the optimized Δ_o values, i.e., $\Delta_o = 0.6$ eV for Co $3d^7$ in CoO, $\Delta_o = 0.8$ eV for Co $3d^6$ in $ZnCo_2O_4$, and $\Delta_o = 0.6$ eV for Co $3d^5$ in $SrCoO_3$. And we use Δ_{eg} $(E_{d3z2-r2} - E_{dx2-y2}) = 2\Delta_{t2g}(E_{dxz,yz} - E_{dxy})$ to parametrize the tetragonal crystal field in the first approximation. Figures 4(a)–4(c) display the simulated spectra at different Δ_{t2g} values ranging from −240 meV to 240 meV with light polarization parallel ($E \parallel c$) and perpendicular ($E \perp c$) to the crystal c axis. Firstly, the simulated spectra show a polarization dependence for $\Delta_{t2g} \neq 0$, indicating a nature linear dichroism. As the crystal field Δ_{t2g} increases, the dichroic effect which is defined as the difference between the absorption spectra calculated for $E \parallel c$ and $E \perp c$ polarizations increases for both positive and negative Δ_{t2g} values, as shown in Figs. 4(e)–4(g). The signs are opposite between positive and negative tetragonal crystal fields for CoO_6 with all three electronic configurations, reflecting perfectly the opposite strain imposed on the corresponding thin films, which, however, are not interchangeable simply by reversing their respective signs due to the orbital symmetry and the multiplet effects.

A comparison of the excitation peak for different linear polarizations reflects the electronic configuration of Co ions. For Co $3d^7$, only one hole exists in the t_{2g} energy level considering the high spin configuration with $\Delta_o = 0.6$ eV. The first excitation peak p_1 corresponds to the transition from $2p$ core level to the lowest empty states of t_{2g} orbitals in the one-electron picture. The hole in t_{2g} shell can be either in d_{xy} or $d_{xz,yz}$ orbitals, the first excitation peak p_1 thus shows strong sensitivity for different photon polarizations. With $\Delta_{t2g} = -240$ meV, a large peak intensity is observed for $E \perp c$ whereas little peak appears for $E \parallel c$ polarization. With $\Delta_{t2g} = 240$ meV, opposite behavior exists with a large peak intensity for $E \parallel c$ polarized incoming wave. With a negative tetragonal crystal field effect ($\Delta_{t2g} < 0$), the t_{2g} orbitals split to low-lying $d_{xz,yz}$ and high-lying d_{xy} energy levels where the former is fully occupied, leaving only the excitation probability for the high-lying d_{xy} orbitals. Due to the parity selection rule, the transition to d_{xy} orbital with $E \parallel c$ photon polarization is forbidden, corresponding to the diminishing excitation peak p_1 intensity for $E \parallel c$ polarized light. In a similar way, unpopulated states only exist in high-lying $d_{xz,yz}$ orbitals for $\Delta_{t2g} > 0$. Peak p_1 intensity almost vanished for $E \perp c$ polarized light. The disappearance of the first excitation peak p_1 in response to different incoming photon polarizations is gradual and increases as the crystal field varies. This can be attributed to the spin-orbit coupling which prefers a spherical charge distribution. Otherwise an abrupt change as Δ_{t2g} switches on is expected if one neglects the spin-orbit coupling. In a similar way, we can understand the changing of the peak intensities with different linear polarizations and the opposite responses of the linear dichroism with opposite tetragonal crystal fields for CoO_6 with $3d^6$ and $3d^5$ electronic configurations, respectively.

D. X-ray linear dichroism and temperature dependent absorption spectra

Besides the splitting of the energy levels with different tetragonal crystal fields that cause the linear dichroic effect, magnetic ordering and exchange field can also give rise to linear dichorism. One of the unique characterization of cobalt oxides is the spin degree of freedom, which is distinctive from other $3d$ transition metal oxides. The magnetic exchange field thus usually needs to be included in cobalt oxides. Figures 5(a)–5(c) show the absorption spectra simulated for CoO_6 $3d^7$, Co $3d^6$, and Co $3d^5$ electronic configurations under cubic symmetry with different linear photon polarizations at an exchange field from 0 meV to 50 meV along out-of-plane direction (crystal c axis). We note that the magnitude of exchange field up to 50 meV considered here covers the exchange field for CoO with $3d^7$ [41,42], $EuCoO_3$ and $LaCoO_3$ with $3d^6$ [2], and $SrCoO_3$ with $3d^5$ [43] at 0 K in literature. As the exchange field switches on, a linear dichorism is clearly visible. With an applied exchange field, both the initial state electron occupation in different orbitals and the final state vary. We note that the linear dichoric spectra for $E \perp c$ and $E \parallel c$ incoming photon polarizations are similar to that originating from positive tetragonal crystal field effects shown in

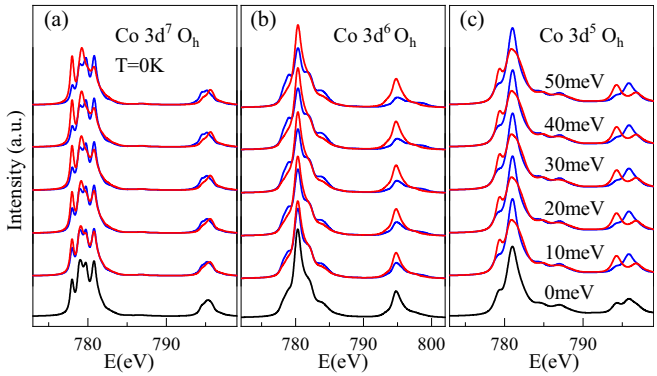

FIG. 5. The calculated Co L_{23}-edge absorption spectra for $E \perp c$ and $E \parallel c$ incoming photon polarizations at 0 K with different exchange field values, i.e., 0 meV, 10 meV, 20 meV, 30 meV, 40 meV, and 50 meV from bottom to top spectra, for (a) Co $3d^7$, (b) Co $3d^6$, and (c) Co $3d^5$ electronic configurations.

Fig. 4. This is because applying an exchange field along the out-of-plane direction favors a preferred orbital momentum along the same direction due to spin-orbit coupling. Taking Co $3d^7$ as an example, only one unpopulated state exists in the $d_{xz,yz}$ orbital level which allows a large intensity with $E \parallel c$ polarized light due to the spin-orbit coupling, whereas the d_{xy} orbital is fully occupied, leaving no transition probability for dipole-allowed transition with $E \perp c$. Therefore, the electronic configuration is the same as positive tetragonal crystal field effect with a lower energy of the d_{xy} orbtial and a high energy for $d_{xz,yz}$ orbitals. As the exchange field increases, the linear dichroism increases for Co $3d^7$. When the exchange field is above the threshold of 30 meV, the linear dichroism varies negligibly. The threshold exchange filed values below are 20 meV and 10 meV for Co $3d^6$ and Co $3d^5$, respectively.

As suggested in Figs. 4 and 5, x-ray linear dichroism shows similar changes due to tetragonal crystal field and magnetic exchange field effect which brings difficulties to explore the underlying mechanism. The question would be how to distinguish them, for which we performed temperature-dependent simulations for CoO_6 clusters with different electronic configurations. The effect of temperature as an external parameter has been considered in present CI cluster calculations through adding the Boltzmann statistics for the state populations; for details we refer to the papers by Haverkort *et al.* [20], Tanaka and Jo [29], and our previous calculations [21,44].

Figure 6 shows the temperature-dependent Co L_3-edge isotropic spectra and the absorption spectra for $E \perp c$ and $E \parallel c$ incoming photon polarizations in the presence of either tetragonal crystal field or magnetic exchange field for Co $3d^7$. The simulated isotropic spectra exhibit negligible temperature dependence at different magnetic exchange fields [Fig. 6(a)] and tetragonal crystal fields [Fig. 6(b)]. However, the polarization-dependent absorption spectra show spectral variations as temperature changes. Figures 6(c)–6(e) show the polarization-dependent simulated spectra at different temperatures, i.e., 20 K, 50 K, 100 K, 150 K, 200 K, and 300 K for magnetic exchange fields $H_{ex} = 10$ meV, 20 meV, and 30 meV, respectively. As temperature rises, the first excitation peak p_1 becomes lower for $E \parallel c$ polarization whereas the intensity of peak p_1 decreases for $E \perp c$ polarization. The temperature here includes two contributions, i.e., the thermal effects which influence the electronic population as temperature increases following the Boltzmann statistics, and the correlated effects due to magnetic exchange interactions or tetragonal lattice distortions. We note that the polarization-dependent simulated spectra with tetragonal crystal field show small changes as temperature varies, as shown in Figs. 6(f)–6(h). Therefore, the polarization-dependent variations in Figs. 6(c)–6(e) are mainly contributed by the magnetic exchange field rather than the tetragonal lattice distortion or the thermal effects.

The simulated spectra for CoO_6 with Co $3d^6$ electronic configuration show different temperature dependence as temperature varies. As shown in Figs. 7(a) and 7(b), the isotropic spectra show small temperature-dependent changes at different exchange fields, whereas the isotropic spectra show strong

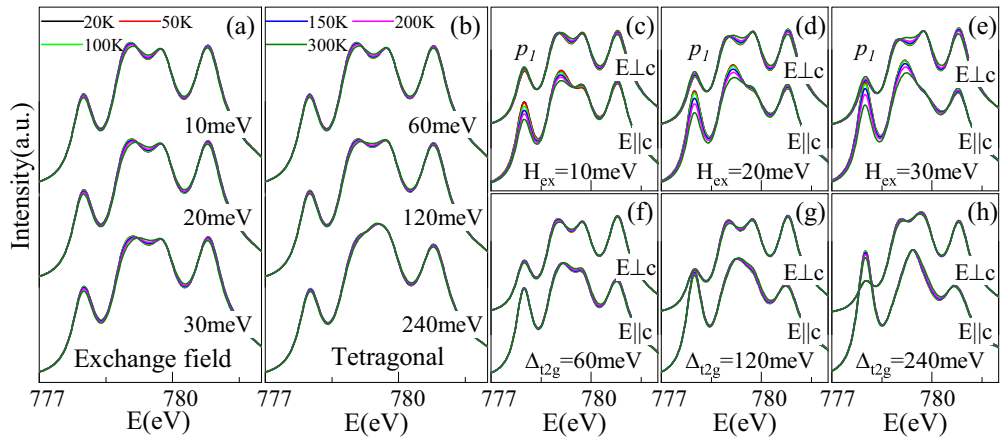

FIG. 6. Temperature-dependent variations of the absorption spectra at Co L_3 edge with Co $3d^7$ electronic configuration. Panel (a) shows the temperature-dependent isotropic spectra for 10 meV, 20 meV, and 30 meV magnetic exchange field. Panel (b) exhibits the temperature-dependent isotropic spectra for tetragonal symmetry with $\Delta_{t2g} = 60$ meV, 120 meV, and 240 meV. Panels (c)–(h) show the temperature-dependent absorption spectra for both $E \parallel c$ and $E \perp c$ incoming photon polarizations in presence of either magnetic exchange fields with $H_{ex} = 10$ meV, 20 meV, and 30 meV or tetragonal crystal fields with $\Delta_{t2g} = 60$ meV, 120 meV, and 240 meV, respectively.

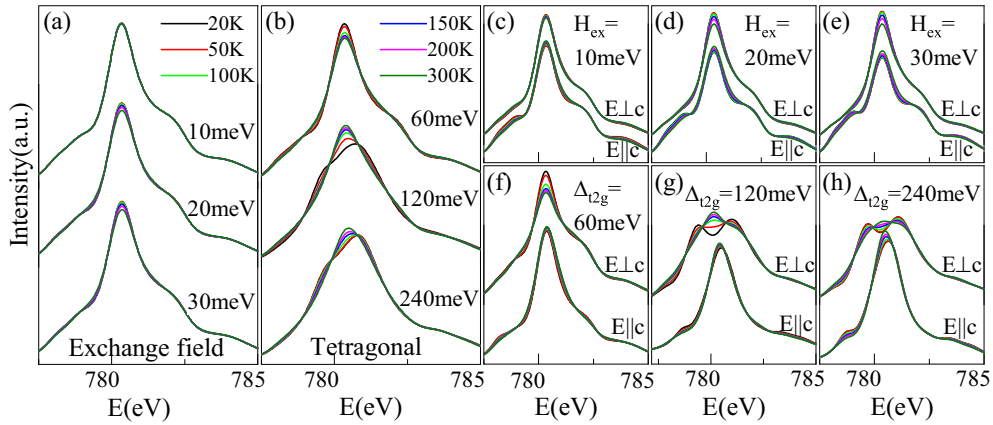

FIG. 7. Panels (a) and (b) show the temperature-dependent isotropic spectra of CoO_6 with Co $3d^6$ electronic configuration for different magnetic exchange fields and tetragonal crystal fields, respectively. Panels (c)–(h) show the temperature-dependent absorption spectra for both $E \parallel c$ and $E \perp c$ polarizations in presence of either magnetic exchange field or tetragonal crystal field, as labeled in the corresponding panel.

spectral variations at different temperatures in the presence of tetragonal crystal fields. Therefore, temperature-dependent absorption measurements will separate the contribution from tetragonal field from magnetic exchange field. The small temperature dependence of Co $3d^6$ with different external H_{ex} suggests that the thermal effect is not dominant here. The simulated spectral variations in Figs. 7(f)–7(h) are mainly contributed by the modification of the ground and final states at different temperatures due to the tetragonal crystal fields. Further polarization-dependent simulations reveal that the temperature-dependent isotropic spectra at different $\Delta_{t2g} =$ 60 meV, 120 meV, and 240 meV mainly originate from the temperature-dependent variations of $E \perp c$ incoming photon polarization.

The simulated spectra for CoO_6 with Co $3d^5$ electronic configuration show similar spectral variations as CoO_6 with $3d^7$ electronic configuration, i.e., the isotropic spectra show negligible temperature dependence, as shown in Figs. 8(a) and 8(b). Moreover, the polarization-dependent absorption spectra exhibit strong temperature dependence for $H_{ex} = 10$ meV, 20 meV, and 30 meV, as shown in Figs. 8(c)–8(e). Overall, temperature- and polarization-dependent absorption measurements can be used to separate the contributions between tetragonal crystal field and magnetic exchange field as well as to understand the ground-state properties.

IV. CONCLUSIONS

In summary, we have grown high-quality epitaxial $ZnCo_2O_4$, $CoAl_2O_4$, and $SrCrO_3$ thin films by pulsed laser deposition technique. Using experimentally measured Co L_{23}-edge absorption spectra as fingerprints, we carried out CI cluster calculations for Co and oxygen ions with local octahedral, tetrahedral, and tetragonal coordination environments. Crystal field splitting between the twofold e_g orbitals and the threefold t_{2g} orbitals exhibits as one of the crucial parameters in determining the optoelectronic properties. Here, we focus on the detailed spectral variations with different octahedral crystal field Δ_o and tetrahedral crystal field Δ_t. The crystal field of a specified compound can be extracted from our simulations, which is important for understanding ground-state properties and is complementary to the results obtained in optical measurements as well as in other calculations. We notice that CI calculations have been intensively studied for CoO_6 clusters with local octahedral coordination, but much

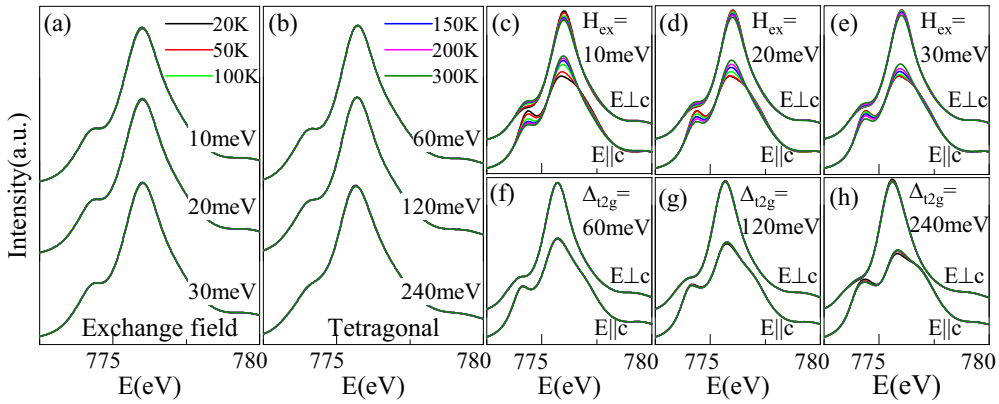

FIG. 8. Panels (a) and (b) show the temperature-dependent isotropic spectra of Co $3d^5$ at different magnetic exchange fields and different tetragonal crystal fields, respectively. Panels (c)–(h) show the temperature-dependent absorption spectra for both $E \parallel c$ and $E \perp c$ polarizations with the specified magnetic exchange or tetragonal crystal field in the corresponding panel.

less for the tetrahedral case in literature. Through a linear combination of the CI simulated spectra with different valences and symmetries, the features of an experimentally measured spectrum of a spinel structure can be well captured. It can work properly for both integer and mixed valence state systems, which is favorable to understand the ground-state properties as well as to explore their multifunctional physical behaviors.

Later, the simulated spectra for CoO_6 clusters in tetragonal symmetry with different incoming photon polarizations revealed the natural linear dichroism. We further showed that the magnetic exchange field can also give rise to linear dichroism, which is necessary to be considered for Co ions with partially filled $3d$ shell and different possible spin states. To separate both contributions, we proposed detailed temperature- and polarization-dependent measurements, which show different spectral variations due to the specified modifications of the ground and final states at different temperatures. Our results offer theoretical guidance for understanding the multiplet structure at Co L_{23}-edge absorption spectra, obtaining the representative energy parameters for comparisons with other measurements or calculations, extracting the precise crystal field for Co oxides with versatile coordinations which determines the optoelectronic applications, and explaining the underlying mechanism of linear dichroism in cobalt oxides and their thin films.

ACKNOWLEDGMENTS

This work was carried out with the support of soft x-ray beamline of Australian Synchrotron and beamline 4B9B of the Beijing Synchrotron Facilities. We acknowledge the financial support by the National Natural Science foundation of China (Grant No. 11704317) and the Fundamental Research Funds for Central Universities (Grant No. 20720210018).

[1] B. Scherrer, A. S. Harvey, S. Tanasescu, F. Teodorescu, A. Botea, K. Conder, A. N. Grundy, J. Martynczuk, and L. J. Gauckler, Phys. Rev. B **84**, 085113 (2011).
[2] G. Zhang, E. Gorelov, E. Koch, and E. Pavarini, Phys. Rev. B **86**, 184413 (2012).
[3] J. A. Alonso, M. J. Martínez-Lope, C. de la Calle, and V. Pomjakushin, J. Mater. Chem. **16**, 1555 (2006).
[4] Y. Li, Y. N. Kim, J. Cheng, J. A. Alonso, Z. Hu, Y.-Y. Chin, T. Takami, M. T. Fernández-Díaz, H.-J. Lin, C.-T. Chen, L. H. Tjeng, A. Manthiram, and J. B. Goodenough, Chem. Mater. **23**, 5037 (2011).
[5] L. Malavasi, C. Tealdi, G. Flor, G. Chiodelli, V. Cervetto, A. Montenero, and M. Borella, Sens. Actuators B **105**, 407 (2005).
[6] R. van Doorn and A. Burggraaf, Solid State Ionics **128**, 65 (2000).
[7] T. Jakubek, W. Kaspera, P. Legutko, P. Stelmachowski, and A. Kotarba, Catal. Commun. **71**, 37 (2015).
[8] J. Buršík, M. Soroka, R. Uhrecký, R. Kuzžel, F. Mika, and S. Huber, Appl. Surf. Sci. **376**, 209 (2016).
[9] Y. Bitla, Y.-Y. Chin, J.-C. Lin, C. N. Van, R. Liu, Y. Zhu, H.-J. Liu, Q. Zhan, H.-J. Lin, C.-T. Chen, Y.-H. Chu, and Q. He, Sci. Rep. **5**, 15201 (2015).
[10] X. C. Huang, J. Y. Zhang, M. Wu, S. Zhang, H. Y. Xiao, W. Q. Han, T.-L. Lee, A. Tadich, D.-C. Qi, L. Qiao, L. Chen, and K. H. L. Zhang, Phys. Rev. B **100**, 115301 (2019).
[11] A. Hassen, A. I. Ali, B. J. Kim, Y. S. Wu, S. H. Park, and B. G. Kim, J. Appl. Phys. **102**, 123905 (2007).
[12] A. Podlesnyak, G. Ehlers, M. Frontzek, A. S. Sefat, A. Furrer, T. Strässle, E. Pomjakushina, K. Conder, F. Demmel, and D. I. Khomskii, Phys. Rev. B **83**, 134430 (2011).
[13] J. van Elp, J. L. Wieland, H. Eskes, P. Kuiper, G. A. Sawatzky, F. M. F. de Groot, and T. S. Turner, Phys. Rev. B **44**, 6090 (1991).
[14] L. Qiao, H. Y. Xiao, H. M. Meyer, J. N. Sun, C. M. Rouleau, A. A. Puretzky, D. B. Geohegan, I. N. Ivanov, M. Yoon, W. J. Weber, and M. D. Biegalski, J. Mater. Chem. C **1**, 4628 (2013).
[15] V. Singh, M. Kosa, K. Majhi, and D. T. Major, J. Chem. Theory Comput. **11**, 64 (2015).
[16] W. Hu, X.-M. Cao, and P. Hu, J. Phys. Chem. C **122**, 19593 (2018).
[17] S. Hu, W. Han, S. Hu, J. Seidel, J. Wang, R. Wu, J. Wang, J. Zhao, Z. Xu, M. Ye, and L. Chen, Chem. Mater. **31**, 6117 (2019).
[18] G. van der Laan, J. Zaanen, G. A. Sawatzky, R. Karnatak, and J.-M. Esteva, Phys. Rev. B **33**, 4253 (1986).
[19] M. W. Haverkort, M. Zwierzycki, and O. K. Andersen, Phys. Rev. B **85**, 165113 (2012).
[20] M. W. Haverkort, Quanty—a quantum many body script language (2016), http://www.quanty.org/.
[21] M. Wu, H. L. Xin, J. O. Wang, X. J. Li, X. B. Yuan, H. Zeng, J.-C. Zheng, and H.-Q. Wang, J. Synchrotron Radiat. **25**, 777 (2018).
[22] M. Wu, J.-C. Zheng, and H.-Q. Wang, Phys. Rev. B **97**, 245138 (2018).
[23] M. Wu, S. Chen, C. Huang, X. Ye, H. Zhou, X. Huang, K. H. L. Zhang, W. Yan, L. Zhang, K. Kim, Y. Du, S. Chambers, J.-C. Zheng, and H.-Q. Wang, Front. Phys. **15**, 13601 (2019).
[24] S. I. Csiszar, M. W. Haverkort, Z. Hu, A. Tanaka, H. H. Hsieh, H.-J. Lin, C. T. Chen, T. Hibma, and L. H. Tjeng, Phys. Rev. Lett. **95**, 187205 (2005).
[25] Z. Hu, H. Wu, M. W. Haverkort, H. H. Hsieh, H. J. Lin, T. Lorenz, J. Baier, A. Reichl, I. Bonn, C. Felser, A. Tanaka, C. T. Chen, and L. H. Tjeng, Phys. Rev. Lett. **92**, 207402 (2004).
[26] M. Taguchi, L. Braicovich, F. Borgatti, G. Ghiringhelli, A. Tagliaferri, N. B. Brookes, T. Uozumi, and A. Kotani, Phys. Rev. B **63**, 245114 (2001).
[27] T. Burnus, Z. Hu, M. W. Haverkort, J. C. Cezar, D. Flahaut, V. Hardy, A. Maignan, N. B. Brookes, A. Tanaka, H. H. Hsieh, H.-J. Lin, C. T. Chen, and L. H. Tjeng, Phys. Rev. B **74**, 245111 (2006).
[28] R. H. Potze, G. A. Sawatzky, and M. Abbate, Phys. Rev. B **51**, 11501 (1995).
[29] A. Tanaka and T. Jo, J. Phys. Soc. Jpn. **63**, 2788 (1994).
[30] S. Samanta, Opt. Mater. (Amsterdam) **45**, 141 (2015).
[31] G. van der Laan and I. W. Kirkman, J. Phys.: Condens. Matter **4**, 4189 (1992).

[32] V. L. Chevrier, S. P. Ong, R. Armiento, M. K. Y. Chan, and G. Ceder, Phys. Rev. B **82**, 075122 (2010).
[33] M. García-Mota, M. Bajdich, V. Viswanathan, A. Vojvodic, A. T. Bell, and J. K. Norskov, J. Phys. Chem. C **116**, 21077 (2012).
[34] N. Hollmann, Z. Hu, M. Valldor, A. Maignan, A. Tanaka, H. H. Hsieh, H.-J. Lin, C. T. Chen, and L. H. Tjeng, Phys. Rev. B **80**, 085111 (2009).
[35] X. C. Huang, W. W. Li, S. Zhang, F. Oropeza, G. Gorni, V. A. de la Pena-O Shea, T.-L. Lee, M. Wu, D. Qi, L. Qiao, J. Cheng, and K. H. L. Zhang (unpublished).
[36] J. H. Haeni, P. Irvin, W. Chang, R. Uecker, P. Reiche, Y. L. Li, S. Choudhury, W. Tian, M. E. Hawley, B. Craigo, A. K. Tagantsev, X. Q. Pan, S. K. Streiffer, L. Q. Chen, S. W. Kirchoefer, J. Levy, and D. G. Schlom, Nature (London) **430**, 758 (2004).
[37] J. M. Rondinelli and N. A. Spaldin, Phys. Rev. B **79**, 054409 (2009).
[38] J. Chakhalian, J. M. Rondinelli, J. Liu, B. A. Gray, M. Kareev, E. J. Moon, N. Prasai, J. L. Cohn, M. Varela, I. C. Tung, M. J. Bedzyk, S. G. Altendorf, F. Strigari, B. Dabrowski, L. H. Tjeng, P. J. Ryan, and J. W. Freeland, Phys. Rev. Lett. **107**, 116805 (2011).
[39] A. Frano, E. Schierle, M. W. Haverkort, Y. Lu, M. Wu, S. Blanco-Canosa, U. Nwankwo, A. V. Boris, P. Wochner, G. Cristiani, H. U. Habermeier, G. Logvenov, V. Hinkov, E. Benckiser, E. Weschke, and B. Keimer, Phys. Rev. Lett. **111**, 106804 (2013).
[40] S. Middey, D. Meyers, S. K. Ojha, M. Kareev, X. Liu, Y. Cao, J. W. Freeland, and J. Chakhalian, Phys. Rev. B **98**, 045115 (2018).
[41] J. Sakurai, W. J. L. Buyers, R. A. Cowley, and G. Dolling, Phys. Rev. **167**, 510 (1968).
[42] M. D. Rechtin and B. L. Averbach, Phys. Rev. B **5**, 2693 (1972).
[43] J. Lim and J. Yu, Phys. Rev. B **98**, 085106 (2018).
[44] M. Wu, J.-C. Zheng, and H.-Q. Wang, J. Appl. Crystallogr. **50**, 576 (2017).